ISSN 1063-7834, Physics of the Solid State, 2018, Vol. 60, No. 12, pp. 2649–2655. © Pleiades Publishing, Ltd., 2018.
Original Russian Text © I.A. Tambasov, A.S. Voronin, N.P. Evsevskaya, M.N. Volochaev, Yu.V. Fadeev, A.S. Krylov, A.S. Aleksandrovskii, A.V. Luk'yanenko, S.R. Abelyan, E.V. Tambasova, 2018, published in Fizika Tverdogo Tela, 2018, Vol. 60, No. 12, pp. 2456–2462.

SURFACE PHYSICS AND THIN FILMS

# Structural and Thermoelectric Properties of Optically Transparent Thin Films Based on Single-Walled Carbon Nanotubes

**I. A. Tambasov[a, *], A. S. Voronin[b], N. P. Evsevskaya[c], M. N. Volochaev[a, d], Yu. V. Fadeev[e], A. S. Krylov[a], A. S. Aleksandrovskii[a, e], A. V. Luk'yanenko[a, e], S. R. Abelyan[a], and E. V. Tambasova[d]**

[a] *Institute of Physics, Siberian Branch, Russian Academy of Sciences, Kransoyarsk, Russia*
[b] *Krasnoyarsk Scientific Center, Siberian Branch, Russian Academy of Sciences, Kransoyarsk, Russia*
[c] *Institute of Chemistry and Chemical Technology, Siberian Branch, Russian Academy of Sciences, Kransoyarsk, Russia*
[d] *Siberian State University of Sciences and Technologies, Krasnoyarsk, Russia*
[e] *Siberian Federal University, Krasnoyarsk, Russia*
**e-mail: tambasov_igor@mail.ru*

Received April 2, 2018; in final form, May 23, 2018

**Abstract**—Thin films have been produced via a spray method from commercially available single-walled carbon nanotubes (SWCNTs). A SWCNT film thickness has ranged from ~10 to ~80 nm. The SWCNT diameter has accepted values of 1.6–1.8 nm. The existence of SWCNTs longer than 10 μm is established. The optimal thickness of a SWCNT thin film is found to be ~15 nm at which the transmittance exceeds 85%. The specific resistance of SWCNT thin films goes from $\sim 1.5 \times 10^{-3}$ to $\sim 3 \times 10^{-3}$ Ohm cm at room temperature. The pioneering study of the temperature dependences of the Seebeck coefficient and surface resistance is performed for this type of SWCNT. A surface resistance is found to increase with rising temperature. Furthermore, the Seebeck coefficient of SWCNT thin films weakly depends on temperature. Its value for all samples is evaluated to be ~40 μV/K. According to the sign of the Seebeck coefficient, thin films exhibit hole-type conductivity. Moreover, the power factor of a 15-nm thin SWCNT-film decreases with a temperature increase to 140°C from the value of approximately ~120 to ~60 μW $m^{-1}$ $K^{-2}$. A further rise in temperature has led to a gain in the power factor.

**DOI:** 10.1134/S1063783418120296

## 1. INTRODUCTION

A huge amount of unused heat energy from industries and other people's livelihoods is released into the environment. Using thermoelectric transducers, a part of heat energy can be converted into electricity. It is worth mentioning that most unused heat energy is at temperatures up to 200°C [1].

The effective conversion of heat into electric energy necessitates materials with outstanding thermoelectric properties, such as hole- or electron-type conductivity $\sigma$ (S $m^{-1}$), a high Seebeck coefficient $S$ (V $K^{-1}$), and the lowest heat conductivity coefficient $\kappa$ (W $m^{-1}$ $K^{-1}$) [2]. The common integral characteristic of thermoelectric materials is thermoelectric Q-factor expressed as $ZT = (S^2\sigma/\kappa)T$, where $T$ is the average temperature between the hot and cool sides of a thermoelectric transducer. The modern studies aimed at searching for and designing materials with excellent thermoelectric properties are thus reduced to meeting these three requirements [2].

Unconditional leaders with the greatest thermoelectric Q-factors at near-room temperatures are compounds based on bismuth and tellurium whose $ZT$ values tend to 1 [3]. Furthermore, these compounds are suitable for the fabrication of materials with hole- or electron-type conductivity. However, their main shortcoming is the use of toxic tellurium, as well as the steady rise in the price of bismuth and tellurium.

In connection with this, flexible electronics became extensively developed to date, aimed at the creation and characterization of flexible thermoelectric transducers [4, 5]. Besides this, the modern science is actively devoted to research and design of nanostructured thermoelectric materials [6–9], mainly due to the ability to tune the thermoelectric Q-factor by changing their structural features [7, 9, 10].

Key materials intended for flexible electronics are various allotropic forms of carbon. Regarding flexible thermoelectric transducers, semiconducting single-walled carbon nanotubes (SWCNTs) seem to be promising candidates for this purpose [11, 12], mainly due to the high Seebeck coefficient [12]. Moreover, their combination with conventional thermoelectric transducers allows one to design and study composite thermoelectric materials in order to achieve good mechanical flexibility and effective thermoelectric conversion. Nowadays, transparent SWCNT-based electrodes are among the promising candidates to be applied instead the transparent conductive oxides in optoelectronics [13], ensuring prospects to implement several functional properties, such as electric conductivity, high optical transparency and thermoelectricity, in the framework of one material. Exhibiting these characteristics, SWCNT thin films seem to be suitable for transparent flexible electronics as the supply sources positioned on a transparent support [14].

There are, however, a very few published works announcing the thermoelectric properties of SWCNT thin films at above room temperatures. It is worth mentioning that state-of-the-art industrial technologies enable one to produce the long SWCNTs at the comparatively low price. Thus, elucidating the thermoelectric properties of thin films based on industrially available SWCNTs has become a relevant task. The present work divulges a pioneering study of optically transparent thin films on the basis of industrially available SWCNTs.

In particular, their thermoelectric properties are monitored within a range of room temperature to 200°C.

## 2. SYNTHESIS AND CHARACTERIZATION OF FILMS

A commercially available SWCNT aerogel ((TUBALL, OCSiAl, Novosibirsk, Russia) was used to prepare aqueous dispersions with SWCNT contents of 0.1 wt %. Thin films were then deposited onto glassy substrates via a spray method as follows.

Compressed air was fed from a compressor to an airbrush under a pressure of 0.6 MPa, nebulizing a SWCNT dispersion onto a heated substrate. The working temperature of a substrate was 130°C. Substrates were heated to avoid the migration of drops and their coalescence. The average drop size in aerosol was 30–50 μm. A distance from an airbrush nozzle to a substrate was 25 cm. A thin film thickness was set by the volume of nebulized SWCNT dispersion.

The contact silver areas were made on a k575x Emitech vacuum setup. Contacts were ~500-nm-thick. The morphology of a thin film surface was probed in a DPN 5000 Nanoink atomic force microscope. A thickness of SWCNT thin films was evaluated in a Hitachi TM7700 transmission electron microscope using the cross-section mode [15, 16].

The optical properties of SWCNT thin films were studied on a Shimadzu UV-3600 spectrometer and on a Horiba Jobin Yvon T64000 Raman spectrometer.

The thermoelectric properties (Seebeck coefficient and conductivity resistance) of thin films were measured from room temperature to 200°C on a self-developed setup equipped with a thermostat, a Keithley 2400 precision current source, a purposely designed sample holder (defining the gradient heating of sample), a pair of K-type thermocouples and a 24-bit LTR114 analog-to-digital converter based on a LTR-EU-2 rack (L Kard Ltd, Russia).

SWCNT thin films were initially rectangles with dimensions of 33 × 25 mm. Two silver contact pads with a width of 4 mm and a length of 25 mm were then applied through a mask via the magnetron sputtering. This resulted in a square SWCNT film with sizes of 25 × 25 mm for measuring the thermoelectric properties. The electric conductivity resistance was evaluated using a two-probe scheme. For this, two clamping probes with silvered and smoothened ends were disposed, one on each silver contact pad of the sample. A SWCNT film sample was placed on a round solid copper table with a diameter of 42 mm and a thickness of 2 mm. The table was fixed in a Specac thermostat operating in the continuous heating mode. The heating rate was ~5 K/min. The continuous heating was a quasi-linear function of time. The temperature was controlled by the two adjacent thermocouples on the sample's surface. The temperature value was taken as a mean of the temperatures from each thermocouple. The conductivity resistance was measured versus temperature by passing a precision steady current $I$ of 50 μA through the contact pads, using a Keithley 2400 current source. The voltage $V$ was also taken from the contact pads by applying a 24-bit LTR114 analog-to-digital transducer based on a LTR-EU-2 rack. The resistance was determined as a ratio of $V/I$. Moreover, the transducer was contemporaneously acquiring data from both thermocouples.

The Seebeck coefficient was measured on a purposely designed holder (Figs. 1a and 1b). The temperature gradient in the continuous heating caused the electric voltage $V_S$ on the contact pads of a sample. The Seebeck coefficient was thus calculated as a ratio of $V_S/\Delta T$, where $\Delta T$ is a difference between the temperatures of the hot and cold sides, respectively. The control and recording of experimental data (conductivity and Seebeck coefficient) were implemented using self-developed software.

## 3. RESULTS AND DISCUSSION

In order to establish the optimal relationship between the optic and thermoelectric properties, the thickness of samples of SWCNT thin films was varied, being ~10, ~15, ~30, ~45, and ~80 nm. Raman spectroscopy is known as a powerful tool for probing structural and electron properties of SWCNTs [17–19]. For this reason, Raman spectroscopy was used in this work to identify the thinnest and the thickest SWCNT thin films. Figure 2 displays the Raman spectra of two samples with thicknesses of 10 and 80 nm.

As seen from Fig. 2, the main lines for both thin films match each other. According to the Raman lines

(a)

(b)

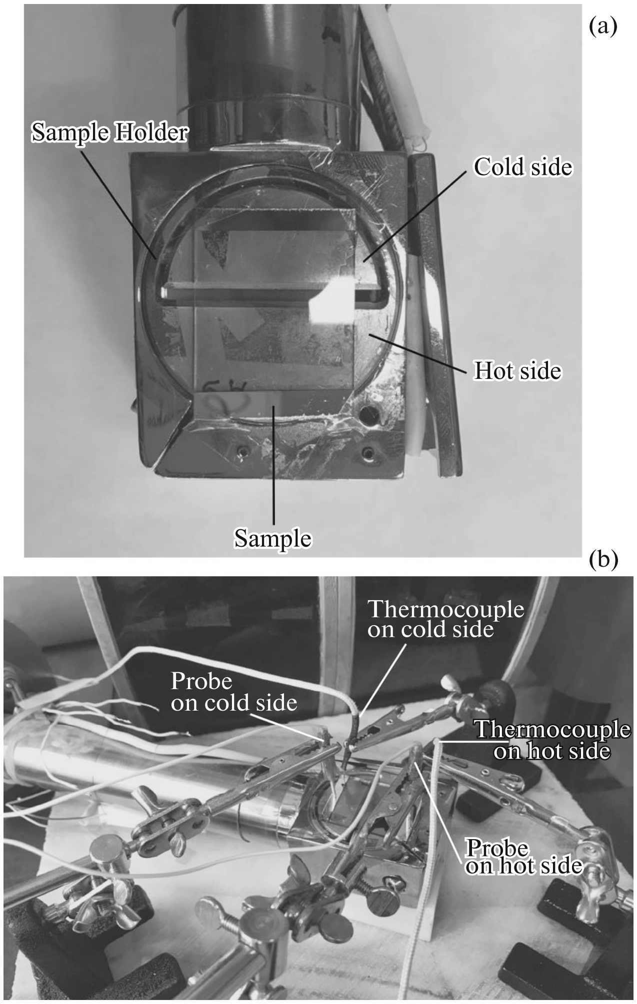


**Fig. 1.** (a) A holder with a sample; (b) the general view of a sample to be subjected to measurements of the Seebeck coefficient.

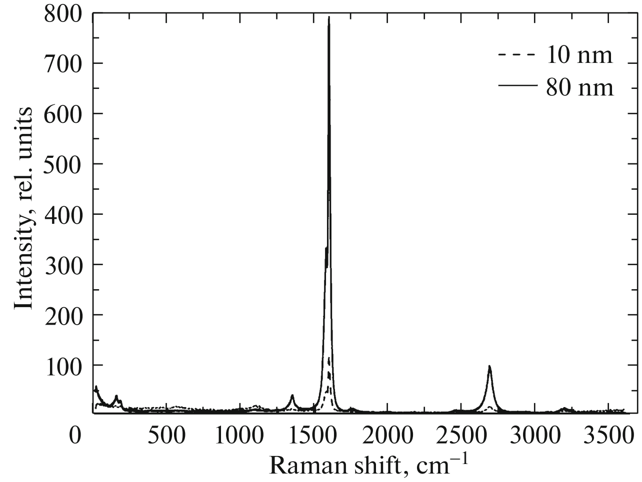


**Fig. 2.** Raman spectrum of 10-nm and 80-nm SWCNT thin film.

in Fig. 1, thin films consist of single-walled carbon nanotubes [18, 20].

The essential information for structural analysis is provided by the radial breathing modes RBM1 (154 $cm^{-1}$) and RBM2 (183 $cm^{-1}$). It is worth noting that individual SWCNTs have a single radial breathing mode. However, the interaction between SWCNTs in the bundle leads to the emergence of two hybrid breathing modes due to the lowering symmetry [18], as observed in SWCNT thin films. So, the dependence given in [21] allows the SWCNT diameters to be estimated as a function of hybrid breathing modes RBM1 (154 $cm^{-1}$) and RBM2 (183 $cm^{-1}$). In our case, the SWCNT diameter ranged from ~1.6 to ~1.8 nm. On the other hand, the SWCNT diameter can be evaluated from the following formula [22]:

$$\omega_{\mathrm{RBM}} = \frac{c_1}{d} + c_2, \qquad (1)$$

where $\omega_{\mathrm{RBM}}$ is the breathing mode of an isolated SWCNT, $c_1$ and $c_2$ are the correction factors and $d$ is a SWCNT diameter. According to [21], the hybrid breathing mode RBM1 is shifted relatively the breathing mode of an isolated SWCNT by 10 $cm^{-1}$. The coefficients $c_1$ and $c_2$ were found in [22] to be 215 $cm^{-1}$ nm and 18 $cm^{-1}$ respectively. Thus, the SWCNT diameter $d$ will be described by the following equation:

$$d = \frac{c_1}{\omega_{\mathrm{RBM}} - c_2}. \qquad (2)$$

Substituting the RBM value of the individual SWCNT (144 $cm^{-1}$), as well as the values of $c_1$ and $c_2$, in Eq. (2) gives the diameter $d = 1.706$ nm. This result matches the earlier found diameter range for SWCNT thin films and coincides with data reported in [23] for the same type of SWCNT.

The Raman spectra also exhibit lines attributed to so-called $D$ (1346 $cm^{-1}$) and $G$ (1593 $cm^{-1}$) vibration modes of SWCNTs [20]. Furthermore, the $G/D$ ratio is frequently used for the qualitative analysis of SWCNTs [24]. Its high value means a small amount of defects in SWCNTs. In this case, the $G/D$ ratio reaches 18.71, which is consistent with values of highly qualitative SWCNTs prepared via various routes [23]. For instance, the $G/D$ ratio for HiPCO SWCNT was found to be 13.8 and that for AD SWCNTs was 52.2 [23].

In order to inspect the morphology and to estimate the SWCNT length in thin films, the surface of samples was scanned via the atomic force microscopy (AFM). The SWCNT length was evaluated in a sample with a SWCNT weight concentration of ~2 × $10^{-4}$ wt % in an aqueous dispersion. Figure 2 shows the AFM images of the surface of SWCNTs in a thin film and of the individual SWCNTs.

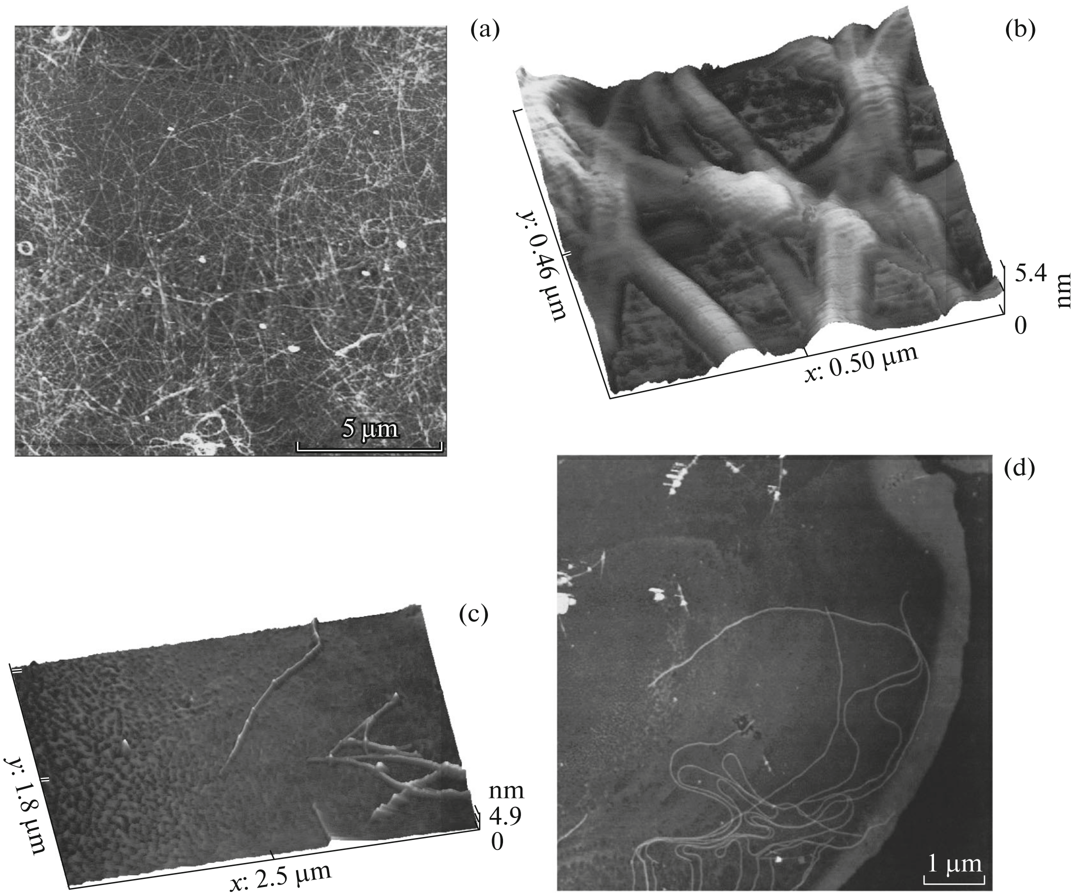


**Fig. 3.** (a) General AFM image of a 10-nm SWCNT thin film; (b) AFM 3D image of the surface of a 10-nm SWCNT thin film; (c) AFM 3D image of the surface of individual short SWCNTs and (d) AFM image of individual long SWCNTs.

As seen in Fig. 3a, SWCNT thin films possess a quite developed surface, with typical bundles of SWCNTs (Fig. 3b). The presence of individual SWCNTs with different lengths is also obvious from Figs. 3c and 3d. Some SWCNTs are shorter than 1 μm (Fig. 3c). At the same time, Fig. 2d highlights the individual SWCNTs with a strongly curved shape and the total length of more than 10 μm. Usually, the SWCNT length depends significantly on the synthesis conditions of a SWCNT dispersion, such as the time and power of the ultrasonic treatment. Carbon materials are known to effectively absorb the optical radiation [25]. For this reason, the optical transmittance was measured versus a thickness of SWCNT thin films in a wavelength range of 200–2500 nm. This dependence is plotted in Fig. 4a. Typically, SWCNTs are the effective broadband light absorbers. As is obvious in Fig. 4a, the transmission spectrum drops within its entire range, when the film thickness is slightly increased. The transmission at a wavelength of 550 nm is also visualized as a function of thin film thickness (Fig. 4b). It is worth mentioning that the transmittance of a glassy substrate was accepted as 100% in the description of the transmittance of SWCNT thin films versus their thickness in Fig. 3b. It is evident from Figs. 4a and 4b that the transmittance at thicknesses above 15 nm goes below 85%. Thus, the thickness of optically transparent SWCNTs thin films must be limited to 15 nm.

To determine the thermoelectric Q-factor of materials, it is essential to study the electric conductivity resistance at various temperatures. In connection with this, the surface resistance of SWCNT thin films was monitored from room temperature to 200°C. The surface resistance was converted into specific one by accounting for the whole film thickness. Note that the room-temperature specific resistance of a 10-nm SWCNT thin film was $\sim 3 \times 10^{-3}$ Ohm cm. On the other hand, the specific resistance for 15-, 30-, 45-, and 80-nm SWCNT thin films was found to be $1.5 \times 10^{-3}$, $\sim 1.8 \times 10^{-3}$, $\sim 1.7 \times 10^{-3}$, and $\sim 1.7 \times 10^{-3}$ Ohm cm, respectively. The discrepancy between specific resistances at small thicknesses is likely due to the loose packing of SWCNTs in comparison with thicker films.

The temperature dependence of the surface resistance exhibits a similar behavior for all samples.

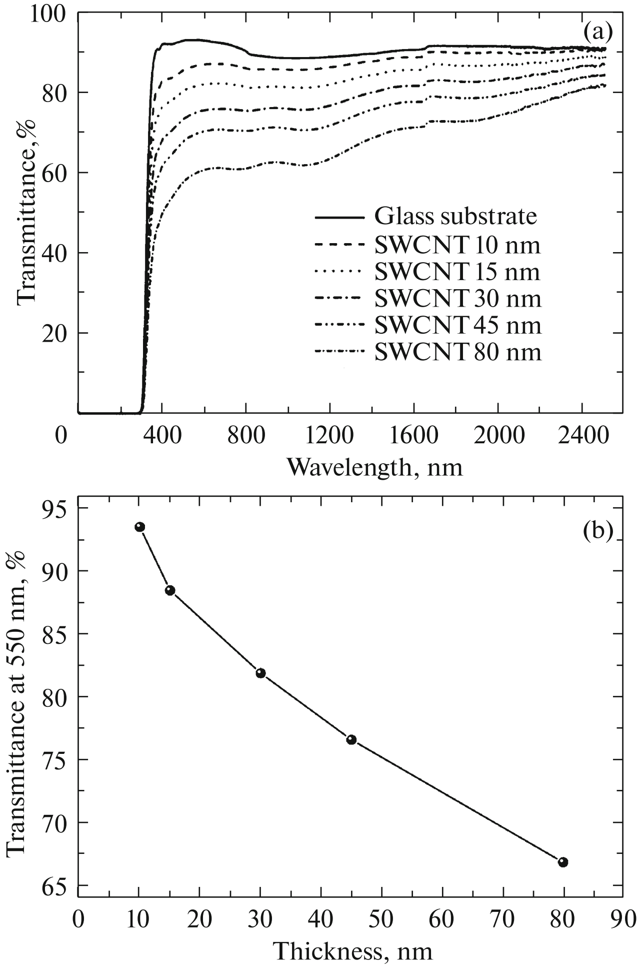


**Fig. 4.** (a) Transmittance spectrum of SWCNT thin films with different thickness on a glassy substrate; (b) optical transmittance at a 550-nm wavelength as a function of SWCNT thin film thickness.

Figure 5 illustrates a typical dependence of the surface resistance of a SWCNT thin film on the temperature. As is seen in Fig. 5, the surface resistance rises with temperature, which is typical to some extent of metals. A similar change in the surface resistance of SWCNT thin films with temperature was observed in [26, 27].

It is shown that the electronic properties of SWCNTs are sensitive to molecules of oxygen and water [28–30] from the environment. These molecules seem to be the complementary acceptors for the electrons in metal SWCNTs at room temperature. The conductivity of SWCNT thin films is mainly due to the holes from semiconducting SWCNTs, because the amount of the latter released upon the synthesis of SWCNTs is about 2/3 [31]. In this respect, the additional acceptors allow the conductivity to be increased in SWCNT thin films. On the other hand, it is likely that an increase in temperature causes the desorption of oxygen and water molecules from the surface of SWCNT thin films. This reduces the amount of acceptors, as well as the conductivity, on account of decreased hole concentration. It has to be mentioned that the above mechanism requires a complementary experimental study.

Figure 6 illustrates the Seebeck coefficient as a function of temperature for a 15-nm SWCNT thin film. As seen, the Seebeck coefficient varies to a small extent for all thin film samples, remaining at the level of ~35–40 μV/K in a whole temperature range. For other samples, the Seebeck coefficient was close to 40 μV/K. Moreover, according to signs of the Seebeck coefficient, all measured materials have the hole-type conductivity. The empirically found Seebeck coefficients match those evaluated earlier for different SWCNTs [31].

One essential integral parameter of thermoelectric materials id the power factor PF (μW m$^{-1}$ K$^{-2}$) expressed, as follows:

$$PF = S^2\sigma. \quad (3)$$

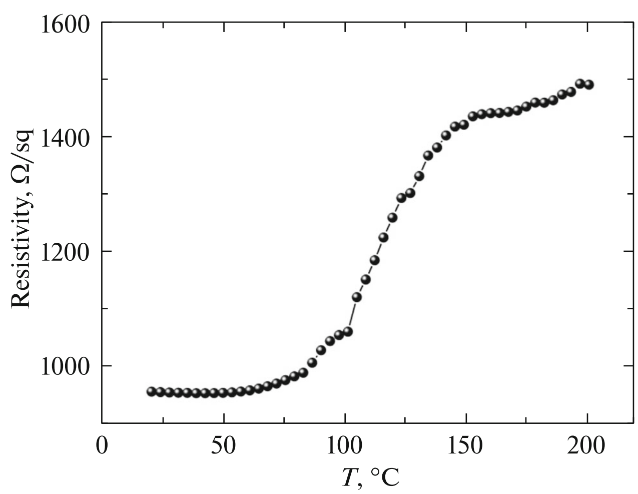


**Fig. 5.** Surface resistance as a function of temperature for a 15-nm SWCNT thin film.

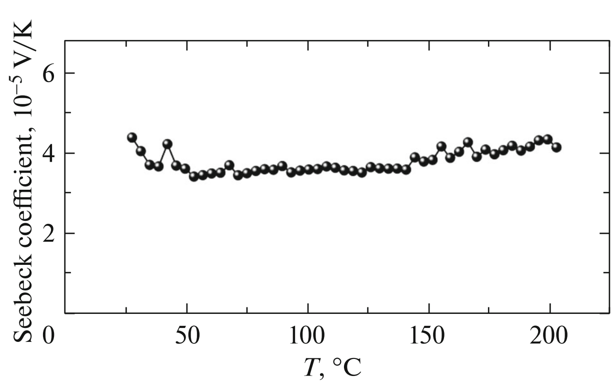


**Fig. 6.** Seebeck coefficient as a function of temperature for a 15-nm SWCNT thin film.

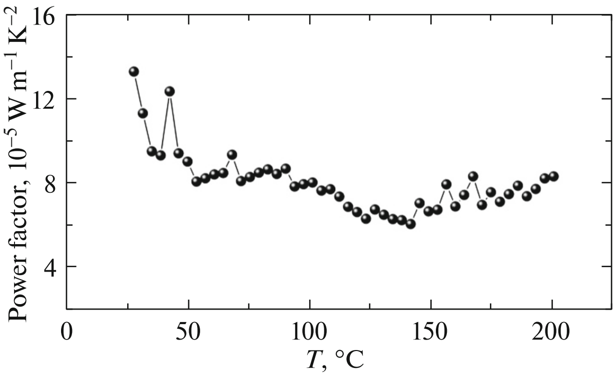


**Fig. 7.** Power factor as a function of temperature for a 15-nm SWCNT thin film.

Formula (3) was used to plot the temperature dependence of the PF for a 15-nm SWCNT thin film (see Fig. 7).

As established, the PF of a 15-nm thin film drops from ~120 to ~60 μW m$^{-1}$ K$^{-2}$ with the temperature increasing to 140°C.However, a further rise in temperature causes a slight increase in PF, and values in this work are found to exceed those for other SWCNTs [31].

Thus, SWCNT thin films seem to be suitable for the design of optically transparent thin-film thermoelectric transducers incorporating the commercially available SWCNTs.

## 4. CONCLUSIONS

SWCNT thin films with variable thickness were prepared of commercially available single-walled carbon nanotubes via a spray method. Their thickness was evaluated using the transmission electron microscopy in the cross-section mode to be 10, 15, 30, 45, and 80 nm respectively. The Raman spectra revealed that the SWCNT diameters ranged from ~1.6 to ~1.8 nm. Furthermore, SWCNTs longer than 10 μm were detected as well.

According to the optical transmittance spectroscopy data, the thicker was the SWCNT film, the lower was the transmittance. The optimal thin film thickness ensuring the transmittance above 85% was therefore found to be below 15 nm.

The room-temperature specific resistance of a 10-nm SWCNT thin film was evaluated to be ~3 × $10^{-3}$ Ohm cm. On the other hand, the specific resistances for 15-, 30-, 45-, and 80-nm thin films were respectively 1.5 × $10^{-3}$, ~1.8 × $10^{-3}$, ~1.7 × $10^{-3}$, and ~1.7 × $10^{-3}$. The different values of specific resistance at small thicknesses seem to be on account of loosely packed SWCNTs as compared to thicker films. Furthermore, the surface resistance was found to increase with temperature. This is likely due to the temperature-induced adsorption of oxygen molecules on the surface of SWCNT thin films.

The Seebeck coefficients of samples remained almost independent of temperature, tending to the value of 40 μV/K. All thin films exhibited the hole-type conductivity in accordance with a sign of the Seebeck coefficient. The power factor for a 15-nm SWCNT thin film dropped from ~120 to ~60 μW m$^{-1}$ K$^{-2}$, while the temperature was increasing to 140°C. However, a further increase in temperature led to a rise in the power factor.

A study of SWCNT thin films is therefore of great importance for the design of optically transparent thin-film thermoelectric transducers incorporating the commercially available SWCNTs.

## ACKNOWLEDGMENTS

This work was supported by the Russian Science Foundation (project no. 17-72-10079).

## REFERENCES

1. N. Toshima, Synth. Met. **225**, 3 (2017).
2. G. J. Snyder and E. S. Toberer, Nat. Mater. 7, **105** (2008).
3. X. Mu, H. Y. Zhou, D. Q. He, W. Y. Zhao, P. Wei, W. T. Zhu, X. L. Nie, H. J. Liu, and Q. J. Zhang, Nano Energy **33**, 55 (2017).
4. D. Madan, Z. Q. Wang, P. K. Wright, and J. W. Evans, Appl Energ. **156**, 587 (2015).
5. Y. N. Chen, Y. Zhao, and Z. Q. Liang, Energ Environ. Sci. **8**, 401 (2015).
6. J. F. Li, W. S. Liu, L. D. Zhao, and M. Zhou, Npg Asia Mater. **2**, 152 (2010).
7. J. He and T. M. Tritt, Science (Washington, DC, U. S.) **357**, 1369 (2017).
8. X. L. Su, P. Wei, H. Li, W. Liu, Y. G. Yan, P. Li, C. Q. Su, C. J. Xie, W. Y. Zhao, P. C. Zhai, Q. J. Zhang, X. F. Tang, and C. Uher, Adv. Mater. **29**, 1602013 (2017).
9. S. Ortega, M. Ibanez, Y. Liu, Y. Zhang, M. V. Kovalenko, D. Cadavid, and A. Cabot, Chem. Soc. Rev. **46**, 3510 (2017).
10. L. D. Hicks and M. S. Dresselhaus, Phys. Rev. B **47**, 12727 (1993).
11. K. Yanagi, S. Kanda, Y. Oshima, Y. Kitamura, H. Kawai, T. Yamamoto, T. Takenobu, Y. Nakai, and Y. Maniwa, Nano Lett. **14**, 6437 (2014).
12. Y. Nakai, K. Honda, K. Yanagi, H. Kataura, T. Kato, T. Yamamoto, and Y. Maniwa, Appl. Phys. Express **7**, 025103 (2014).
13. A. P. Tsapenko, A. E. Goldt, E. Shulga, Z. I. Popov, K. I. Maslakov, A. S. Anisimov, P. B. Sorokin, and A. G. Nasibulin, Carbon **130**, 448 (2018).
14. C. Yang, D. Souchay, M. Kneiss, M. Bogner, M. Wei, M. Lorenz, O. Oeckler, G. Benstetter, Y. Q. Fu, and M. Grundmann, Nat. Commun. **8**, 16076 (2017).

15. I. A. Tambasov, A. S. Tarasov, M. N. Volochaev, M. V. Rautskii, V. G. Myagkov, L. E. Bykova, V. S. Zhigalov, A. A. Matsynin, and E. V. Tambasova, Phys. E (Amsterdam, Neth.) **84**, 162 (2016).
16. V. G. Myagkov, L. E. Bykova, A. A. Matsynin, M. N. Volochaev, V. S. Zhigalov, I. A. Tambasov, Y. L. Mikhlin, D. A. Velikanov, and G. N. Bondarenko, J. Solid State Chem. **246**, 379 (2017).
17. M. S. Dresselhaus, G. Dresselhaus, A. Jorio, A. G. Souza, and R. Saito, Carbon **40**, 2043 (2002).
18. T. Belin and F. Epron, Mater. Sci. Eng. B **119**, 105 (2005).
19. M. S. Dresselhaus, A. Jorio, M. Hofmann, G. Dresselhaus, and R. Saito, Nano Lett. **10**, 751 (2010).
20. M. S. Dresselhaus and P. C. Eklund, Adv. Phys. **49**, 705 (2000).
21. L. Henrard, V. N. Popov, and A. Rubio, Phys. Rev. B **64**, 205403 (2001).
22. J. Maultzsch, H. Telg, S. Reich, and C. Thomsen, Phys. Rev. B **72**, 205438 (2005).
23. A. Chortos, I. Pochorovski, P. Lin, G. Pitner, X. Z. Yan, T. Z. Gao, J. W. F. To, T. Lei, J. W. Will, H. S. P. Wong, and Z. N. Bao, ACS Nano **11**, 5660 (2017).
24. V. M. Irurzun, M. P. Ruiz, and D. E. Resasco, Carbon **48**, 2873 (2010).
25. A. A. Ivanenko, I. A. Tambasov, A. A. Pshenichnaia, and N. P. Shestakov, Opt. Mater. **73**, 388 (2017).
26. B. B. Parekh, G. Fanchini, G. Eda, and M. Chhowalla, Appl. Phys. Lett. **90**, 121913 (2007).
27. D. Kim, H. C. Lee, J. Y. Woo, and C. S. Han, J. Phys. Chem. C **114**, 5817 (2010).
28. P. S. Na, H. J. Kim, H. M. So, K. J. Kong, H. J. Chang, B. H. Ryu, Y. M. Choi, J. O. Lee, B. K. Kim, J. J. Kim, and J. H. Kim, Appl. Phys. Lett. **87**, 093101 (2005).
29. P. G. Collins, K. Bradley, M. Ishigami, and A. Zettl, Science (Washington, DC, U. S.) **287**, 1801 (2000).
30. A. Zahab, L. Spina, P. Poncharal, and C. Marliere, Phys. Rev. B **62**, 10000 (2000).
31. J. L. Blackburn, A. J. Ferguson, C. Cho, and J. C. Grunlan, Adv. Mater. **30**, 1704386 (2018).

*Translated by O. Maslova*